Molecular Immunology 109 (2019) 108–115

Contents lists available at ScienceDirect

Molecular Immunology

journal homepage: www.elsevier.com/locate/molimm

Transcriptome sequencing to unravel the molecular mechanisms underlying the cuticle liquefaction of *Antheraea pernyi* following *Antheraea pernyi* nucleopolyhedrovirus challenge

Guobao Wang, Shuang Na, Xiaoxia Duan, Zheming Leng, Yiren Jiang, Shenglin Shi, Ruisheng Yang, Li Qin*

College of Bioscience and Biotechnology, Liaoning Engineering & Technology Research Center for Insect Resources, Shenyang Agricultural University, Shenyang, 110866, China

ARTICLE INFO

Keywords:
Antheraea pernyi
ApNPV
Cuticle
Chitin
Liquefaction

ABSTRACT

Baculovirus causes liquefaction of insect cuticle to enhance the dissemination of progeny virions away from the host cadavers for increasing viral transmission rates. *Antheraea pernyi* nucleopolyhedrovirus (ApNPV) infects *A. pernyi* larvae with circular pus blotches formed in cuticle in the early stage of liquefaction. To investigate the formation mechanism of those pus blotches, the transcriptome profile changes of the cuticles between ApNPV-infected and non-infected *A. pernyi* larvae were analyzed using RNA-Seq. The transcriptome was *de novo* assembled using the Trinity platform. Comparison of gene expression levels revealed that a total of 2990 and 4427 unigenes were up- and down-regulated respectively in ApNPV-infected cuticle, of which 2620 and 1903 differentially expressed genes (DEGs) could be enriched in different GO terms and KEGG pathways. In this study, we focused on chitin metabolism related DEGs, and screened 10 genes involved in chitin synthesis and degradation with down-regulated trends, indicating that the chitin metabolism pathway was inhibited by ApNPV infection, which may promote liquefaction of *A. pernyi* cuticle. Besides, we also identified a large number of DEGs involved in immune related pathways via KEGG analysis, indicating that intense immune responses occurred in *A. pernyi* cuticle. Our research findings will serve as a basis for further researching the molecular mechanisms underlying cuticle liquefaction of *A. pernyi* induced by ApNPV infection.

1. Introduction

Insect cuticles form an exoskeleton which covers the surface of insect body, and play important roles in numerous physiological functions to protect the body from invasion of pathogens, physical injury and dehydration (Li et al., 2017). The cuticle is a more or less rigid structure due to the presence of chitin and sclerotized proteins (Togawa et al., 2004; Deng et al., 2016). Chitin is one of the most important biopolymers in nature. The great strength and stability of this amino polysaccharide underlie its essential roles in maintaining the specific morphology of insects and resisting invasion of pathogens (Merzendorfer et al., 2003a; Merzendorfer, 2011). It has been demonstrated that chitin in insect cuticle could be degraded by several baculovirus enconding enzymes including chitinase and cathepsin protease in the late stage of infection (Ohkawa et al., 1994; Slack et al., 1995; Hawtin et al., 1997; Kang et al., 1998; Merzendorfer et al., 2003b; Wang et al., 2005), which causes the subsequent liquefaction of cuticle, thus enhances the dissemination of progeny virions away from the host cadavers (Hodgson et al., 2011). However, a detailed report about the molecular mechanisms underlying the cuticle liquefaction in host insect infected with baculovirus is lacking.

Antheraea pernyi nuclear polyhedrosis, which is caused by *A. pernyi* nucleopolyhedrovirus (ApNPV) infection, causes enormous damage to the sericulture industry (Li et al., 2016). ApNPV has high infectivity to cells of multiple tissues of *A. pernyi* larvae, including fat body, hemolymph, trachea, and dermis. In the infection stage of 5th instar *A. pernyi* larvae, the body segment of infected larvae swellings, and the liquefaction process is initiated with various sizes of circular pus blotches in the subcutaneous tissue of the verrucous protuberance which is located at cuticle are observed, and such blotches spread to the entire cuticle tissue at the late stage. Finally, the cuticle of infected larvae ruptures to release virus particles and causes the death of larvae. In this study, RNA-sequencing (RNA-Seq) was employed to investigate the formation mechanism of pus blotches in *A. pernyi* cuticle infected with ApNPV at

* Corresponding author at: College of Bioscience and Biotechnology, Shenyang Agricultural University, No. 120 Dongling Road, Shenyang, 110866, China.
E-mail address: qinli1963@163.com (L. Qin).

https://doi.org/10.1016/j.molimm.2019.03.009
Received 23 January 2019; Received in revised form 21 February 2019; Accepted 19 March 2019
Available online 27 March 2019
0161-5890/

Fig. 1. (A) ApNPV-infected *A. pernyi* larva. (B) Non-infected *A. pernyi* larva. Bar = 1 cm.

the gene expression level. The transcriptome sequences were *de novo* assembled. We systematically analyzed the gene expressional profiles and obtained both up- and down-regulated genes in ApNPV-infected cuticle compared with control. Meanwhile, we screened the chitin metabolism-related differentially expressed genes (DEGs) from the transcriptome data, and further characterized those DEGs based on their expression profiles challenged by ApNPV. Our research findings lay the foundation for further research on the molecular mechanisms of liquefaction induced by viral infection in insect.

2. Materials and methods

2.1. Treatment with ApNPV and cuticle collection

The *A. pernyi* strain, Jiaolan, stored in our laboratory was used in this study. The larvae were fed with fresh leaves of *Quercus liaotungensis* at 23 ± 2 °C with 70 ± 5% relative humidity. The newly molted 5th instar larvae were separated into two groups randomly with twenty in each group. Each larva in experimental group was fed with leaves added with a viral suspension of ApNPV (4.05×10^6 polyhedra/mL) (Li et al., 2016), which with 0.9% physiological saline (150 mmol/L NaCl) in control group. Cuticles were dissected from *A. pernyi* larvae in the two groups at 120 h post infection (Fig.1) and stored at -80 °C for further use.

Table 2
Unigenes annotated in different databases.

Database	Number of unigenes	Ratio (%)
All	39874	100.00
GO	9427	23.64
KEGG	6514	16.34
Pfam	9979	25.03
Swiss-Prot	8442	21.17
eggNOG	13364	33.52
NCBI_nr	13971	35.04

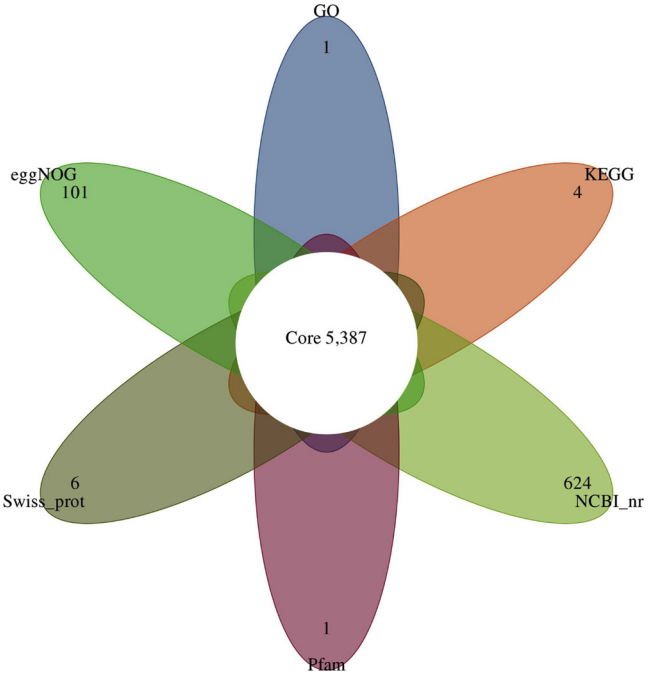

Fig. 2. Petal map of unigenes annotated in NCBI_nr, GO, KEGG, Swiss-Prot, Pfam, Swiss-Prot, and eggNOG databases.

2.2. Total RNA extraction, cDNA library construction and Illumina RNA-Seq

Total RNA was extracted using Trizol reagent (Invitrogen) according to the manufacturer's protocol. The quantity and purity of RNA were analyzed using Bioanalyzer 2100 and RNA 6000 Nano LabChip Kit (Agilent, CA, USA). Approximately 10 μg of total RNA was subjected to isolate Poly (A) mRNA with poly-T oligo-attached magnetic beads (Invitrogen). Following purification, the poly(A)- or poly(A)+ RNA fractions is fragmented into small pieces using divalent cations under elevated temperature. Then the cleaved RNA fragments were reverse-transcribed to create the final cDNA library in accordance with the protocol for the mRNA-Seq sample preparation kit (Illumina, San Diego, USA), the average insert size for the paired-end libraries was 300 bp

Table 1
Statistical analysis of the transcriptome sequence data.

Sample	Raw reads	Raw bases	Valid reads	Valid bases	Valid%	Q20%	Q30%	GC%
ApNPV-infected_1	57332226	8.60G	55715544	8.00G	97.18	96.96	92.14	45.62
ApNPV-infected _2	48859400	7.33G	48130252	7.07G	98.51	98.32	95.47	45.49
ApNPV-infected _3	50197630	7.53G	49354556	7.24G	98.32	98.20	95.23	45.37
Control_1	52086538	7.81G	51102012	7.51G	98.11	98.32	95.45	47.49
Control_2	52447736	7.87G	51633978	7.59G	98.45	98.33	95.46	47.78
Control_3	47585326	7.14G	46798094	6.88G	98.35	98.38	95.59	47.68

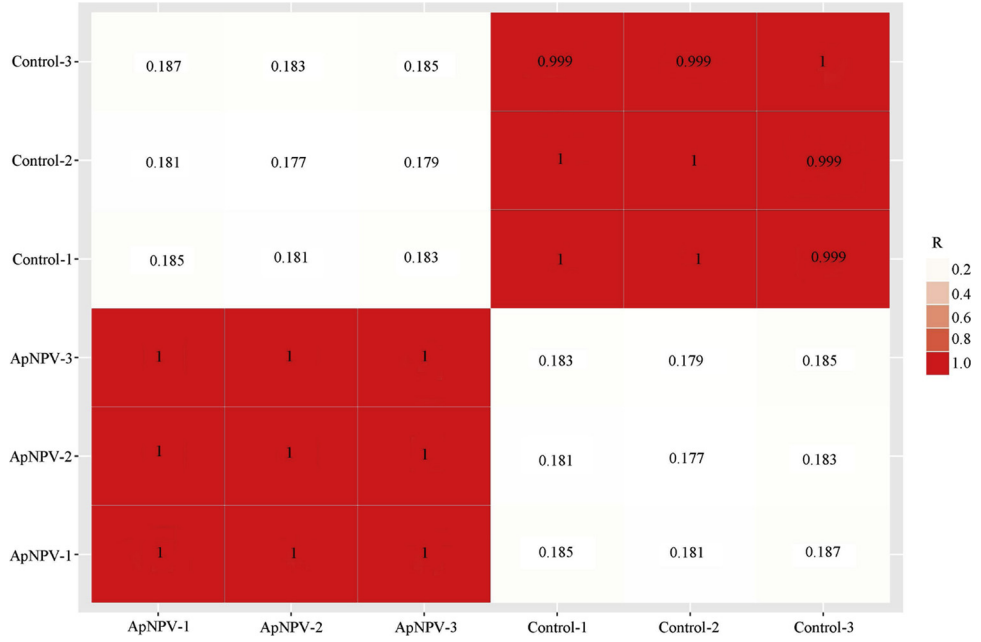

Fig. 3. Pearson correlation between the samples in ApNPV-infected and control groups.

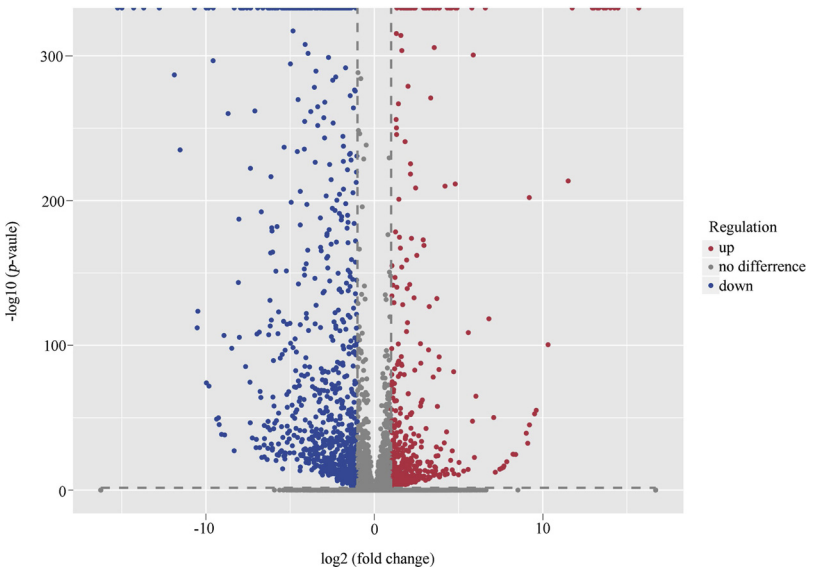

Fig. 4. Volcano plot of the DEGs. The horizontal ordinate represents the fold change of gene expression in the different experimental groups, and the vertical ordinate represents the statistical significance of the change of gene expression. Each point in the plot represents each gene, and the red and blue points represent the significant up- and down-regulated genes (For interpretation of the references to colour in this figure legend, the reader is referred to the web version of this article).

(± 50 bp). And then the paired-end sequencing was performed on an Illumina Hiseq 4000 (lc-bio, China).

2.3. De novo transcriptome assembly

The clean reads were filtered from the raw reads by removing the reads containing adaptor contamination, low quality bases and undetermined bases using Cutadapt and perl scripts in house (Martin, 2011). The sequence quality including the Q20, Q30 and GC-content of the clean data was verified using FastQC (http://www.bioinformatics.babraham.ac.uk/projects/fastqc/). All downstream analyses were based on clean data of high quality. The transcriptome was *de novo* assembled with Trinity 2.4.0 (Grabherr et al., 2011), which groups transcripts into clusters based on shared sequence content. Such a transcript cluster is very loosely referred to as a 'unigene'. The longest transcript in the cluster was chosen as the 'unigene' sequence. The Salmon mothed (Patro et al., 2017) was used to perform expression level for unigenes by calculating TPM (Mortazavi et al., 2008). The differentially expressed unigenes were selected with $\log_2$ (fold change) > 1 or $\log_2$ (fold change) < -1 and with statistical significance (p-value < 0.05) by R package edger (Robinson et al., 2010).

2.4. Unigene annotation and functional classification

All assembled unigenes were aligned against the non-redundant (Nr) protein database (http://www.ncbi.nlm.nih.gov/), Gene ontology (GO) (http://www.geneontology.org), SwissProt (http://www.expasy.ch/sprot/), Kyoto Encyclopedia of Genes and Genomes (KEGG) (http://www.genome.jp/kegg/) and eggNOG (http://eggnogdb.embl.de/) databases using DIAMOND (Buchfink et al., 2015) with a threshold of E-value < 0.00001. Phylogenetic analysis was performed using MEGA 6 software with the neighbor-joining method (Tamura et al., 2013). GO and KEGG enrichment analysis were again performed on the differentially expressed unigenes by perl scripts in house.

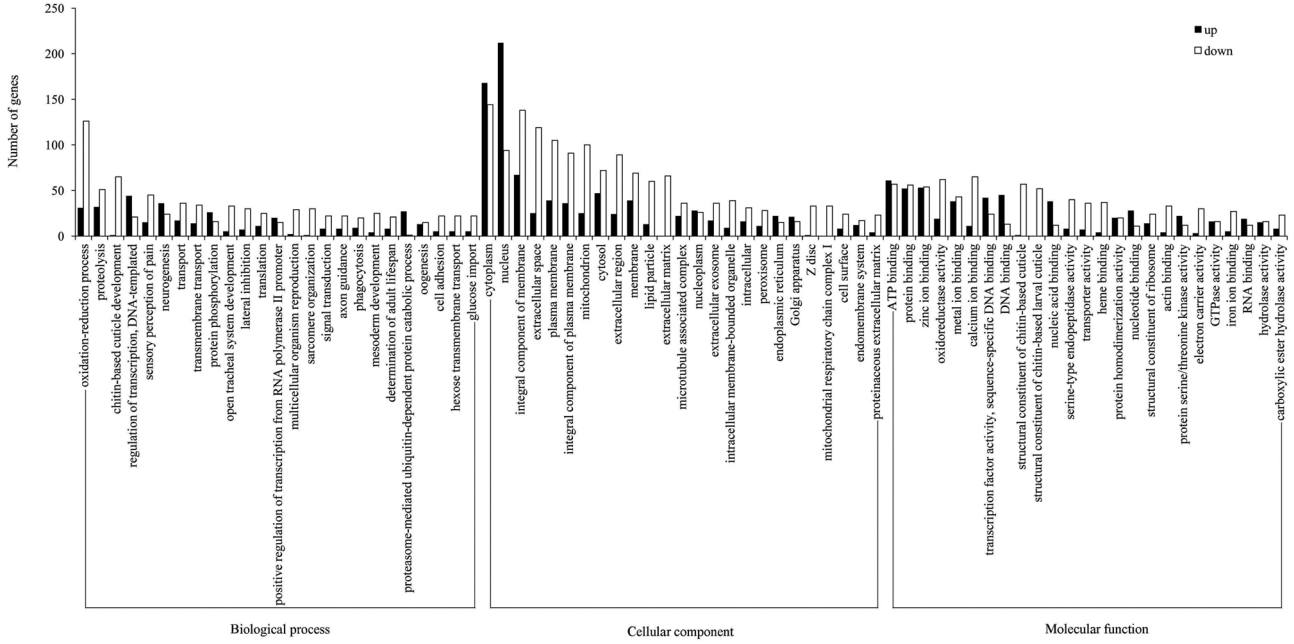

Fig. 5. The top 25 GO terms in cellular component, molecular function and biological process categories with the DEGs enriched in. Black and white bars indicate up- and down-regulated genes respectively.

2.5. Validation of RNA-Seq by quantitative RT-PCR

Sixteen DEGs, including 7 up- and 9 down-regulated genes, were selected for qRT-PCR to validate the transcriptome data. Total RNA from the control and ApNPV-infected samples used for qRT-PCR were the same as for RNA-Seq. The gene-specific primers were designed using the predicted CDSs as reference sequences. qRT-PCR was performed on a CFX Connect™ Real-Time System (Bio-Rad) using a 20 μL reaction system with a procedure as follows: 95 °C for 30 s, followed by 39 cycles of 95 °C for 5 s, 60 °C for 30 s. Melting curves were generated after each run to confirm a single PCR product. Each reaction was run in triplicate. mRNA quantity of each gene was calculated with the $2^{-\Delta\Delta CT}$ method (Livak and Schmittgen, 2001) and normalized to the *A. pernyi* housekeeping gene, *Apactin1* (GenBank: GKC242321.1). The primers used in this study were provided in Table S1.

3. Results

3.1. Summary of RNA-Seq

RNA samples from the cuticles of the two groups (ApNPV-infected and control) were sequenced with three replicates included in each group. The RNA-seq data generated 57332226, 48859400, 50197630 and 52086538, 52447736, 47585326 raw reads from ApNPV-infected and control groups, respectively (Table1). After data filtering, 55715544, 48130252, 49354556, 51102012, 51633978, 46798094 clean reads were obtained (Table1). The raw sequence reads have been deposited in the Gene Expression Omnibus (GEO) under the accession number GSE125821. Using the Trinity *de novo* assembly programme, all short-read sequences were assembled into 87036 transcripts and 50126 unigenes (Table S2). All assembled unigenes were aligned against different protein databases. As shown in Table2, a total of 39874 unigenes with 9427, 6514, 9979, 8442, 13364, and 13971 matched to GO, KEGG, Pfam, Swiss-Prot, eggNOG, and NCBI_nr, respectively (Fig.2, Table S3-S8), and 5387 unigenes could be annotated in all six databases.

3.2. The pearson correlation between different samples

The pearson correlation between different samples in ApNPV-infected and control groups was detected. The correlation coefficient of the three repeats between each other in ApNPV-infected group were all 1, which were 0.999 and 1 between different repeats in the control group (Fig.3), indicating the high similarity of gene expression patterns between different samples in the two groups respectively.

3.3. Analysis of DEGs

With fold changes of > 2 or < 0.5 and FDR < 0.05, 7417 DEGs were identified from the ApNPV-infected group compared with the control, including 2990 up- and 4427 down-regulated genes (Table S9). The distribution of the DEGs was shown in Fig. 4. GO assignments were used to assign a functional classification to these DEGs. A total of 2620 DEGs including 983 up- and 1637 down-regulated genes were assigned into three main categories: biological process, cellular component and molecular function with 2524, 534 and 1166 GO terms respectively (Table S10). The top 25 significantly enriched GO terms of the DEGs for each category were shown in Fig. 5. For the biological process category, the DEGs were mainly assigned to oxidation-reduction process, proteolysis, and chitin-based cuticle development. In cellular component, the most enriched GO terms of the DEGs were cytoplasm, nucleus, integral component of membrane, and extracellular space. The largest subcategory of molecular function was binding, such as ATP binding, protein binding, and zinc ion binding.

All DEGs were assigned to the biochemical pathways described in KEGG and the results showed that 1903 DEGs including 709 up- and 1194 down-regulated genes, were assigned to 282 KEGG pathways (Table S11). For the up-regulated genes, the most enriched pathways were proteasome, ubiquitin mediated proteolysis, and endocytosis (Fig. 6A), which were oxidative phosphorylation, carbon, retinol and purine metabolism, lysosome, phagosome, and peroxisome for the down-regulated genes separately (Fig. 6B).

3.4. Validation of the transcriptome data reliability by qRT-PCR

The expression profiles of *A. pernyi* housekeeping gene, *Apactin1*, in

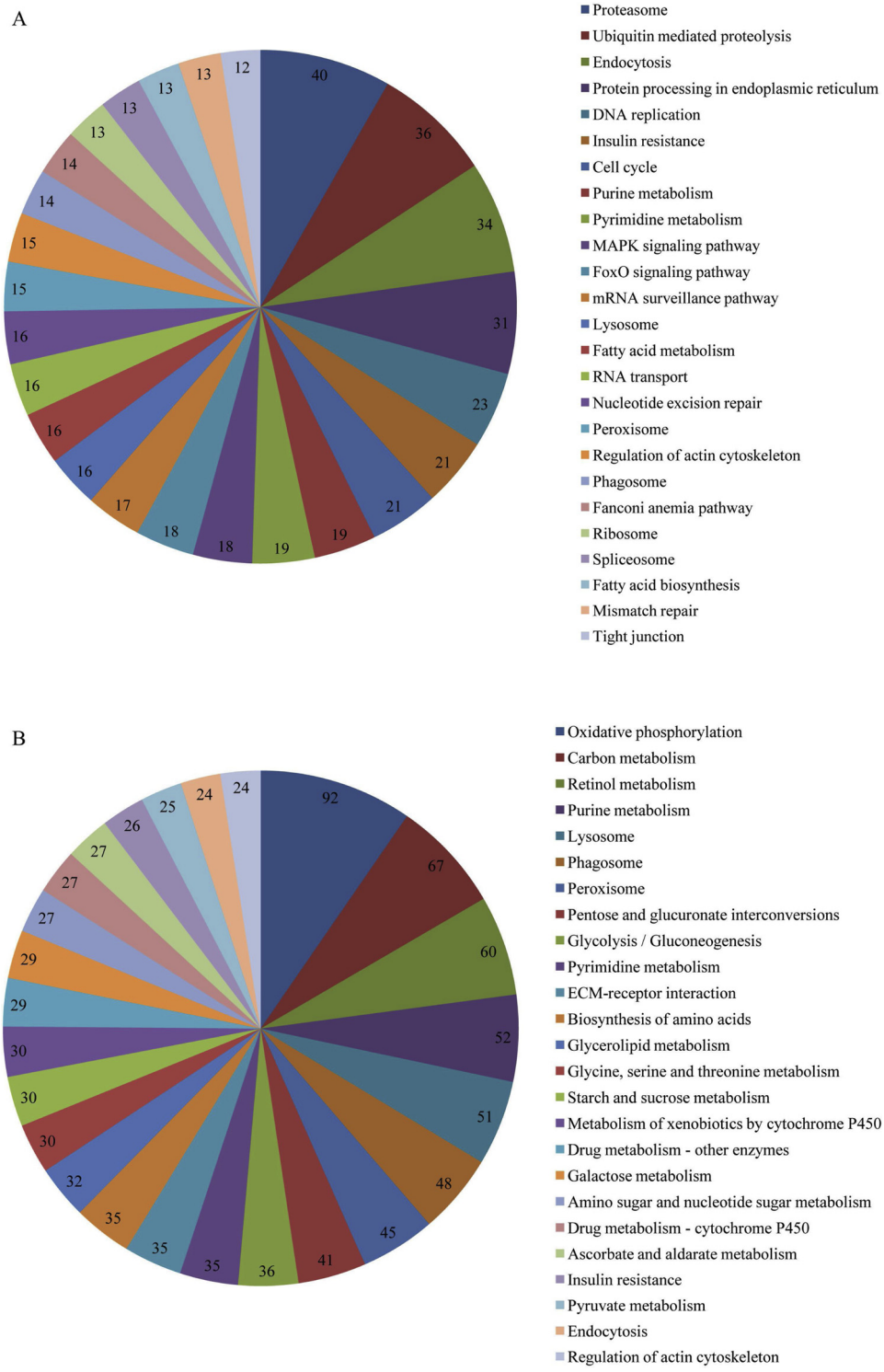

Fig. 6. (A) The top 25 enriched pathways for the up-regulated genes. (B) The top 25 enriched pathways for the down-regulated genes.

ApNPV-infected and control groups were detected. The results showed that almost no difference in expression of *Apactin1* existed between the two groups (data was not shown). Then we selected 16 DEGs including 9 related to chitin metabolism and 7 involved in immune response related pathways of *A. pernyi* for qRT-PCR verification to validate the reliability of the transcriptome data. The results showed that the expression patterns of the candidate genes were consistent with those from RNA-seq (Fig. 7), which confirmed that the RNA-seq data were suitable for further analysis.

4. Dissusion

Baculovirus infection causeing liquefaction of host tissues has been observed in several insect species, including *Bombyx mori*, *Autographa california*, and *Antheraea pernyi*. Unlike other insects, various sizes of circular pus blotches appear on the cuticle of *A. pernyi* at the liquefaction stage (Fig.1). To investigate the molecular mechanisms underlying the pus blotches formation, transcriptome sequencing was used to compare the genes in the ApNPV-infected cuticle that were

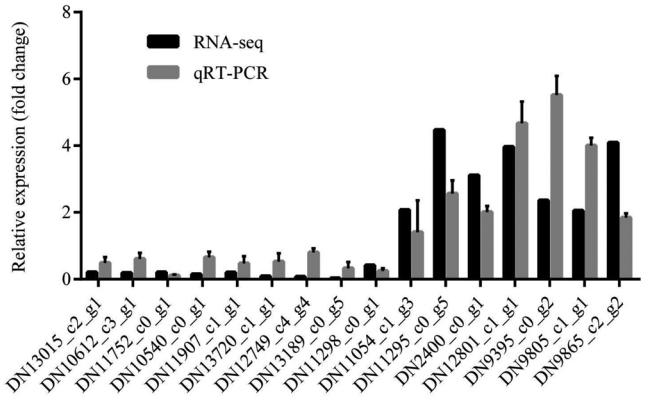

Fig. 7. qRT-PCR verification of RNA-seq data. X- and Y-axis represent the 16 selected DEGs and the relative expression respectively. DN13015_c2_g1, PREDICTED: hexokinase type 2 isoform X1 [*Papilio polytes*]. DN10612_c3_g1, PREDICTED: putative hexokinase HKDC1 [*Bombyx mori*]. DN11752_c0_g1, phosphoglucose isomerase [*Melitaea cinxia*]. DN10540_c0_g1, PREDICTED: glutamine–fructose-6-phosphate aminotransferase [isomerizing] 1-like [*Amyelois transitella*]. DN11907_c1_g1, glucosamine-6-phosphate N-acetyltransferase [*Bombyx mori*]. DN13720_c1_g1, chitin synthase [*Manduca sexta*]. DN12749_c4_g4, chitin deacetylase [*Helicoverpa armigera*]. DN13189_c0_g5, chitinase 7 [*Spodoptera exigua*]. DN11298_c0_g1, chitinase 2 [*Cnaphalocrocis medinalis*]. DN11054_c1_g3, saposin-like protein [*Bombyx mori*], DN11295_c0_g5, PREDICTED: lipase 3-like [*Bombyx mori*]. DN2400_c0_g1, phosphatidylinositol 3-kinase 60 [*Bombyx mori*]. DN12801_c1_g1, cysteine proteinase inhibitor precursor [*Manduca sexta*]. DN9395_c0_g2, PREDICTED: serine/threonine-protein kinase PAK 3 [*Bombyx mori*]. DN9805_c1_g1, PREDICTED: tyrosine-protein kinase transmembrane receptor Ror2 [*Amyelois transitella*]. DN9865_c2_g2, dual specificity protein phosphatase 18 [*Operophtera brumata*].

differentially expressed relative to the control, and a total of 7417 DEGs were identified. In this study, we focused on the chitin metabolism related DEGs.

Chitin degradation is a leading cause for cuticle liquefaction in insects. The biosynthetic pathway for insect chitin synthesis starting with trehalose and ending with the chitin polymer. From the RNA-seq data, several DEGs encoding enzymes involved in this catalytic process with down-regulated trends were obtained, including DN13015_c2_g1 and DN10612_c3_g1, DN11752_c0_g1, DN10540_c0_g1, DN11907_c1_g1, and DN13720_c1_g1 encoding hexokinase, glucose-6-phosphate isomerase, glutamine-fructose-6-phosphate aminotransferase, glucosamine-6-phosphate N-acetyltransferase, and chitin synthase respectively (Table 3). Among those enzymes, chitin synthase (CHS) is definitely the key enzyme within the biosynthetic pathway. CHS is an integral membrane glycosyltransferase that is essential for chitin chain polymerization and deposition in insect chitinous structures. Two CHS classes have been identifed in insects: CHSAs are specifically expressed in the cuticle and related ectodermal cells such as tracheal cells, whereas chitin associated with peritrophic matrice is synthesized by CHSBs (Tellam et al., 2000; Arakane et al., 2005; Bolognesi et al., 2005; Merzendorfer, 2006). We performed phylogenetic analysis of *A. pernyi* chitin synthase (DN13720_c1_g1) identified from the transcriptome data, and the results showed that ApCHS formed a cluster with *Manduca sexta*chitin synthase 1 (MsCHS1) (Fig.8) which belongs to CHSA (Merzendorfer and Zimoch, 2003b), suggesting that ApCHS was classified into CHSA which is responsible for biosynthesis of the chitin found in cuticle. The down-regulation of the chitin synthesis-related enzymes (Table 3) indicated that the biosynthetic pathway of chitin in *A. pernyi* cuticle was inhibited by ApNPV infection.

In insects, chitin synthases and chitinolytic enzymes work hand in hand in remodeling chitinous structures. Among the enzymes playing roles in chitin metabolism, chitin deacetylase (CDA) has been identified as the protein that catalyzes the conversion of chitin into chitosan, thereby modifying the physical properties of insect cuticles and peritrophic matrices (Tsigos et al., 2000). The CDA regulated deacetylation could increase the solubility and decrease the density of chitin fibrils, and influence their structure and orientation in the cuticle (Zhao et al., 2010). Insect chitinases belong to family 18 glycosylhydrolases, and are predicted to mediate the digestion of chitin present in the exoskeleton and peritrophic membrane to chitooligosaccharides (Kramer and Muthukrishnan, 1997). Based on amino acid sequence similarity and the presence or absence of specific domains and conserved sequences, insect chitinases could be grouped into eight unique groups with different domain architectures (Zhu et al., 2004, (Zhu et al., 2008)2008; Arakane and Muthukrishnan, 2009) [28–30]. We screened 2 DEGS (DN13189_c0_g5, DN11298_c0_g1) encoding chitinases based on GO and conversed domain analysis in ApNPV-infected cuticle, and 1 DEG encoding CDA (DN12749_c4_g4) with down-regulated trends (Table 3), suggesting the inhibition of ApNPV on the enzyme activities of those chitinases. According to the classifications of Chen et al. (2017) and the results of phylogenetic analysis in this study, the two *A. pernyi* chitinases encoded by DN13189_c0_g5 and DN11298_c0_g1 were classified into Group III and Group VII respectively (Fig.9).

Additionally, we also screened a large number of DEGs involved in immune response related pathways in the cuticle of *A. pernyi* challenged by ApNPV from the results of KEGG pathway analysis. A total of 262 DEGs were enriched in cellular immunity related pathways including regulation of autophagy, endocytosis, lysosome, phagosome, apoptosis and ubiquitin mediated proteolysis, and 98 DEGs enriched in MAPK signaling pathway, complement and coagulation cascades, Toll-like receptor signaling pathway, Jak-STAT signaling pathway, melanogenesis and insulin signaling pathway which are involved in humoral immunity (Table S11), indicating that intense immune responses occurred in *A. pernyi* cuticle after ApNPV infection. In conclusion, the findings of the present study provide new clues for further exploring the molecular mechanisms of liquefaction in *A. pernyi* cuticle caused by ApNPV infection.

Acknowledgements

This work was supported by the Scientific Research Project for Education Department of Liaoning Province (No. LSNYB201613), the

Table 3
The DEGs involved in chitin metabolism in *A. pernyi* cuticle.

Gene ID	Annotation	log2FC	Regulation
DN13015_c2_g1	PREDICTED: hexokinase type 2 isoform X1 [*Papilio polytes*]	−2.24	down
DN10612_c3_g1	PREDICTED: putative hexokinase HKDC1 [*Bombyx mori*]	−2.43	down
DN11752_c0_g1	glucose-6-phosphate isomerase [*Drosophila simulans*]	−2.23	down
DN10540_c0_g1	PREDICTED: glutamine-fructose-6-phosphate aminotransferase [isomerizing] 1-like [*Amyelois transitella*]	−2.73	down
DN11907_c1_g1	glucosamine-6-phosphate N-acetyltransferase [*Bombyx mori*]	−2.34	down
DN13720_c1_g1	chitin synthase [*Manduca sexta*]	−3.52	down
DN12749_c4_g4	chitin deacetylase [*Helicoverpa armigera*]	−3.59	down
DN13189_c0_g5	chitinase 7 [*Spodoptera exigua*]	−4.97	down
DN11298_c0_g1	chitinase 2 [*Cnaphalocrocis medinalis*]	−1.24	down

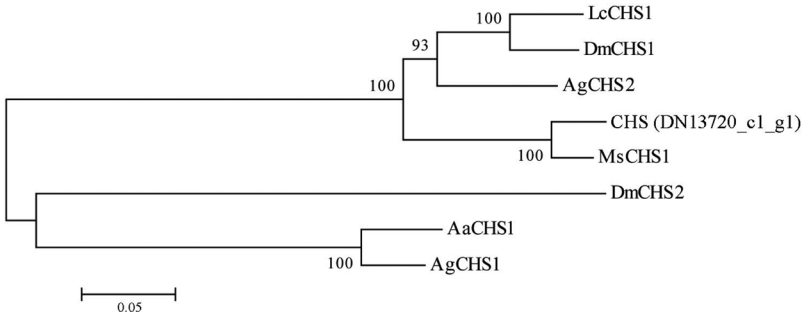

Fig. 8. Phylogenetic analysis of ApCHS and selected chitin synthases. ClustalW software was used to perform multiple sequence alignments prior to phylogenetic analysis Neighbor-joining tree were constructed using MEGA 6 software with 1000-fold bootstrap resampling. The numbers at the nodes of the branches represent the level of bootstrap support for each branch. The species and the chitin synthase sequences followed by their accession numbers are listed as follows: *Manduca sexta*(MsCHS1, AY062175.2). *Lucilia cuprina* (LcCHS1, AF221067.1). *Aedes aegypti* (AaCHS1, AF223577.2). *Drosophila melanogaster* (DmCHS1, NM_079509.3; DmCHS2, NM_079485.4). *Anopheles gambiae* (AgCHS1, AY056833.1; AgCHS2, XM_321336.5).

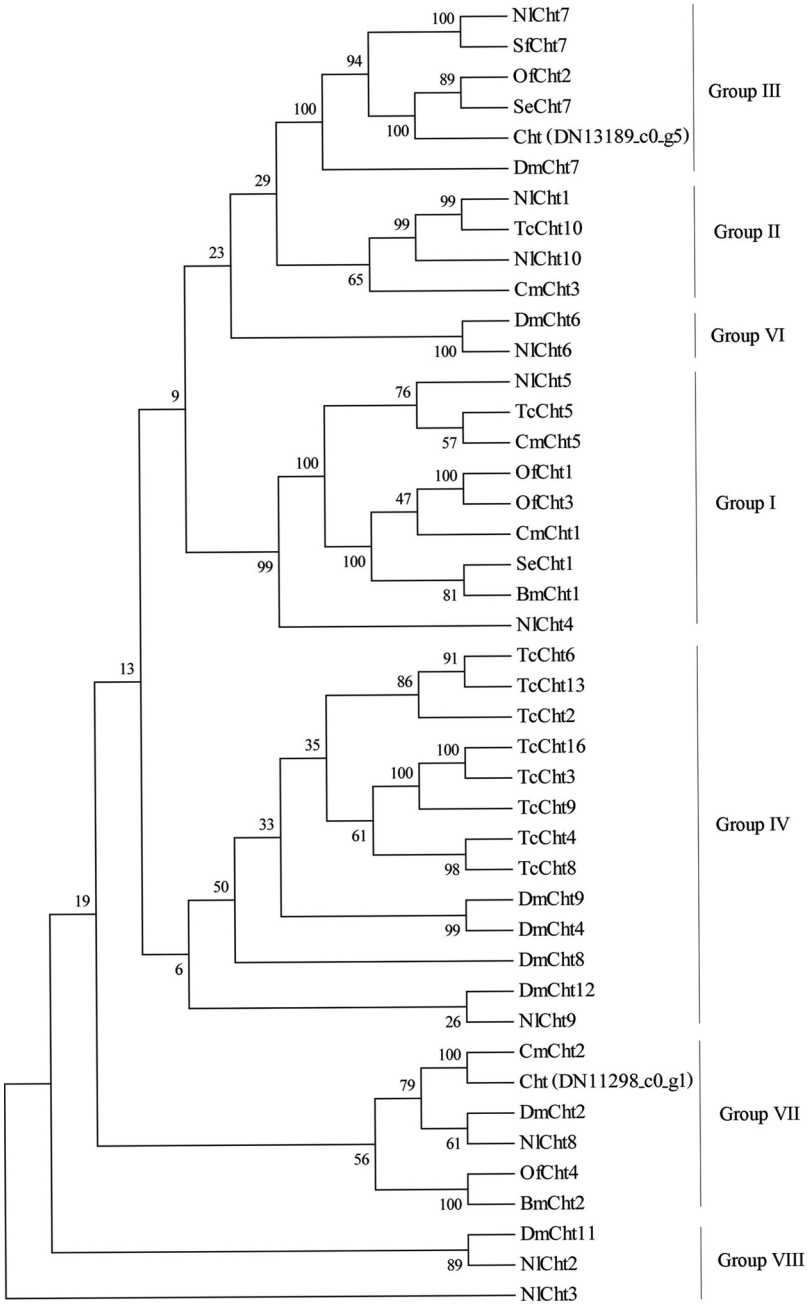

Fig. 9. Phylogenetic tree of chitinases from eight insect species. The tree was generated using MEGA6 software with Neighbor-joining methods. Bootstrap analyses of 1000 replicates were performed and bootstrap values represented in cladograms. Amino acid sequences of chitinases from different insect species were chosen for analysis. The following insect chitinase sequences were used: *Bombyx mori* (Bm), *Drosophila melanogaster* (Dm), *Nilaparvata lugens* (Nl), *Tribolium castaneum* (Tc), *Ostrinia furnacalis* (Of), *Spodoptera exigua* (Se), *Sogatella furcifera* (Sf), *Cnaphalocrocis medinalis* (Cm). Sequences (GenBank accession numbers) used were as follows: BmCht1 (AAG37105.1), BmCht2 (BAC67246.1), DmCht2 (NP_477298.2), DmCht4 (AAF46664.2), DmCht6 (NP_001245599.1), DmCht7 (NP_647768.3), DmCht8 (AAF46663.2), DmCht9 (AAF46665.3), DmCht11 (NP_572361.1), DmCht12 (AAM68191.1), NlCht1 (AJO25036.1), NlCht2 (AJO25037.1), NlCht3 (AJO25038.1), NlCht4 (AJO25039.1), NlCht5 (AJO25040.1), NlCht6 (AJO25041.1), NlCht7 (AJO25042.1), NlCht8 (AJO25043.1), NlCht9 (AJO25044.1), NlCht10 (AJO25045.1), TcCht2 (AAW67569.2), TcCht3 (AAW67570.1), TcCht4 (ABL73927.1), TcCht5 (AAV74190.1), TcCht6 (AAW67572.1), TcCht8 (ABG47446.1), TcCht9 (ABG47447.1), TcCht10 (ABG47448.1), TcCht13 (ABG47450.1), TcCht16 (AAW67571.2), OfCht1 (AAW50396.1), OfCht2 (AGX32025.1), OfCht3 (ABB97081.2), OfCht4 (BAE16587.1), SeCht1 (AAV91784.1), SeCht7 (AFM38213.1), SfCht7 (ARE59262.1), CmCht1 (AII78788.1), CmCht2 (AJG44542.1), CmCht3 (AJG44543.1), CmCht5 (AJG44545.1).

Liaoning Province Doctor Startup Fund (No. 20170520270), and the National Modern Agriculture Industry Technology System Construction Project (Silkworm and Mulberry) (CARS-18).

Appendix A. Supplementary data

Supplementary material related to this article can be found, in the online version, at doi:https://doi.org/10.1016/j.molimm.2019.03.009.

References

Arakane, Y., Muthukrishnan, S., 2009. Insect chitinase and chitinase-like proteins. Cell. Mol. Life Sci. 67 (2), 201–216.

Arakane, Y., Muthukrishnan, S., Kramer, K.J., Specht, C.A., Tomoyasu, Y., Lorenzen, M.D., Kanost, M., Beeman, R.W., 2005. The *Tribolium* chitin synthase genes TcCHS1 and TcCHS2 are specialized for synthesis of epidermal cuticle and midgut peritrophic matrix. Insect Mol. Biol. 14 (5), 453–463.

Bolognesi, R., Arakane, Y., Muthukrishnan, S., Kramer, K.J., Terra, W.R., Ferreira, C., 2005. Sequences of cDNAs and expression of genes encoding chitin synthase and chitinase in the midgut of Spodoptera frugiperda. Insect Biochem. Mol. Biol. 35 (11), 1249–1259.

Buchfink, B., Xie, C., Huson, D.H., 2015. Fast and sensitive protein alignment using DIAMOND. Nat. Methods 12 (1), 59–60.

Chen, C., Yang, H., Tang, B., Yang, W., Jin, D., 2017. Identification and functional analysis of chitinase 7 gene in white-backed planthopper, Sogatella furcifera. Comp. Biochem. Physiol. B, Biochem. Mol. Biol. 208–209 19-28.

Deng, H.M., Li, Y., Zhang, J.L., Liu, L., Feng, Q.L., 2016. Analysis of expression and chitin-binding activity of the wing disc cuticle protein BmWCP4 in the silkworm. Bombyx mori. Insect Sci. 23 (6), 782–790.

Grabherr, M.G., Haas, B.J., Yassour, M., Levin, J.Z., Thompson, D.A., Amit, I., Adiconis, X., Fan, L., Raychowdhury, R., Zeng, Q., Chen, Z., Mauceli, E., Hacohen, N., Gnirke, A., Rhind, N., di Palma, F., Birren, B.W., Nusbaum, C., Lindblad-Toh, K., Friedman, N., Regev, A., 2011. Full-length transcriptome assembly from RNA-Seq data without a reference genome. Nat. Biotechnol. 29 (7), 644–652.

Hawtin, R.E., Zarkowska, T., Arnold, K., Thomas, C.J., Gooday, G.W., King, L.A., Kuzio, J.A., Possee, R.D., 1997. Liquefaction of *Autographa californica* nucleopolyhedrovirus-infected insects is dependent on the integrity of virus-encoded chitinase and cathepsin genes. Virology. 238 (2), 243–253.

Hodgson, J.J., Arif, B.M., Krell, P.J., 2011. Interaction of *Autographa californica* multiple nucleopolyhedrovirus cathepsin protease progenitor (proV-CATH) with insect baculovirus chitinase as a mechanism for proV-CATH cellular retention. J. Virol. 85 (8), 3918–3929.

Kang, W., Tristem, M., Maeda, S., Crook, N.E., O'Reilly, D.R., 1998. Identification and characterization of the *Cydia pomonella* granulovirus cathepsin and chitinase genes. J. Gen. Virol. 79 (9), 2283–2292.

Kramer, K.J., Muthukrishnan, S., 1997. Insect chitinases: molecular biology and potential use as biopesticides. Insect Biochem. Mol. Biol. 27 (11), 887–900.

Li, X.S., Wang, G.B., Sun, Y., Liu, W., He, Y.Z., Wang, F.C., Jiang, Y.R., Qin, L., 2016. Transcriptome analysis of the midgut of the Chinese oak silkworm *Antheraea pernyi* infected with *Antheraea pernyi* nucleopolyhedrovirus. PLoS One 11 (11), e0165959.

Li, Z.L., Tian, S., Yang, H., Zhou, X., Xu, S.P., Zhang, Z.Y., Gong, J., Hou, Y., Xia, Q.Y., 2017. Genome-wide identification of chitin-binding proteins and characterization of BmCBP1 in the silkworm. Bombyx mori. Insect Sci. https://doi.org/10.1111/1744-7917.12552.

Livak, K.J., Schmittgen, T.D., 2001. Analysis of relative gene expression data using real-time quantitative PCR and the $2^{-\triangle\triangle Ct}$ method. Methods. 25 (4), 402–408.

Martin, M., 2011. Cutadapt removes adapter sequences from high-throughput sequencing reads. Embnet J. 17 (1), 10–12.

Merzendorfer, H., 2006. Insect chitin synthases: a review. J Comp Physiol B. 176 (1), 1–15.

Merzendorfer, H., 2011. The cellular basis of chitin synthesis in fungi and insects: common principles and differences. Eur. J. Cell Biol. 90 (9), 759–769.

Merzendorfer, H., Zimoch, L., 2003a. Chitin metabolism in insects: structure: function and regulation of chitin synthases and chitinases. J. Exp. Biol. 206 (Pt 24), 4393–4412.

Merzendorfer, H., Zimoch, L., 2003b. Chitin metabolism in insects: structure, function and regulation of chitin synthases and chitinases. J. Exp. Biol. 206 (Pt 24), 4393–4412.

Mortazavi, A., Williams, B.A., McCue, K., Schaeffer, L., Wold, B., 2008. Mapping and quantifying mammalian transcriptomes by RNA-Seq. Nat. Methods 5 (7), 621–628.

Ohkawa, T., Majima, K., Maeda, S., 1994. A cysteine protease encoded by the baculovirus *Bombyx mori* nuclear polyhedrosis virus. J. Virol. 68 (10), 6619–6625.

Patro, R., Duggal, G., Love, M.I., Irizarry, R.A., Kingsford, C., 2017. Salmon provides fast and bias-aware quantification of transcript expression. Nat. Methods 14 (4), 417–419.

Robinson, M.D., McCarthy, D.J., Smyth, G.K., 2010. EdgeR: a bioconductor package for differential expression analysis of digital gene expression data. Bioinformatics. 26 (1), 139–140.

Slack, J.M., Kuzio, J., Faulkner, P., 1995. Characterization of v-cath, a cathepsin L-like proteinase expressed by the baculovirus *Autographa californica* multiple nuclear polyhedrosis virus. J. Gen. Virol. 76 (Pt5), 1091–1098.

Tamura, K., Stecher, G., Peterson, D., Filipski, A., Kumar, S., 2013. MEGA6: molecular evolutionary genetics analysis version 6.0. Mol. Biol. Evol. 30 (12), 2725–2729.

Tellam, R.L., Vuocolo, T., Johnson, S.E., Jarmey, J., Pearson, R.D., 2000. Insect chitin synthase-cDNA sequence, gene organization and expression. Eur. J. Biochem. 267 (19), 6025–6042.

Togawa, T., Nakato, H., Izumi, S., 2004. Analysis of the chitin recognition mechanism of cuticle proteins from the soft cuticle of the silkworm. Bombyx mori. Insect Biochem Mol Biol. 34 (10), 1059–1067.

Tsigos, I., Martinou, A., Kafetzopoulos, D., Bouriotis, V., 2000. Chitin deacetylases: new, versatile tools in biotechnology. Trends Biotechnol. 18 (7), 305–312.

Wang, F., Zhang, C.X., Shyam Kumar, V., Wu, X.F., 2005. Influences of chitinase gene deletion from BmNPV on the cell lysis and host liquefaction. Arch. Virol. 150 (5), 981–990.

Zhao, Y., Park, R.D., Muzzarelli, R.A., 2010. Chitin deacetylases: properties and applications. Mar. Drugs 8 (1), 24–46.

Zhu, Q., Deng, Y., Vanka, P., Brown, S.J., Muthukrishnan, S., Kramer, K.J., 2004. Computational identification of novel chitinase-like proteins in the *Drosophila melanogaster* genome. Bioinformatics. 20 (2), 161–169.

Zhu, Q., Arakane, Y., Banerjee, D., Beeman, R.W., Kramer, K.J., Muthukrishnan, S., 2008. Domain organization and phylogenetic analysis of the chitinase like family of proteins in three species of insects. Insect Biochem Mol. Biol. 38 (4), 452–466.